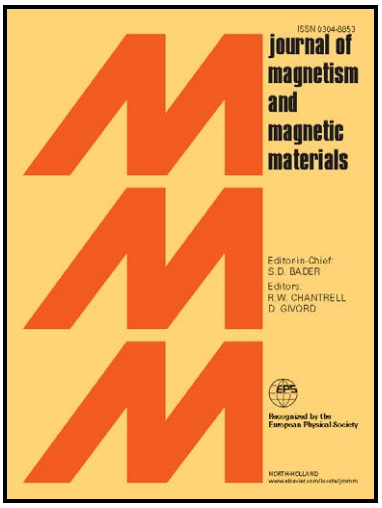

Magnetic second-harmonic generation from interfaces and nanostructures

J.F. McGilp, L. Carroll, K. Fleischer, J.P. Cunniffe, S. Ryan

PII: S0304-8853(09)00387-4
DOI: doi:10.1016/j.jmmm.2009.03.081
Reference: MAGMA 55433

To appear in: *Journal of Magnetism and Magnetic Materials*

Received date: 22 October 2008
Accepted date: 31 March 2009

Cite this article as: J.F. McGilp, L. Carroll, K. Fleischer, J.P. Cunniffe and S. Ryan, Magnetic second-harmonic generation from interfaces and nanostructures, *Journal of Magnetism and Magnetic Materials* (2009), doi:10.1016/j.jmmm.2009.03.081

Magnetic second-harmonic generation from interfaces and nanostructures

J.F. McGilp*, L. Carroll, K. Fleischer, J.P. Cunniffe and S. Ryan

School of Physics, Trinity College Dublin, Dublin 2, Ireland

*Corresponding author. Tel.: +353 18961733; fax: +353 16711759. E-mail address: jmcgilp@tcd.ie

Abstract

Magneto-optic techniques provide non-contact and non-destructive characterization of magnetic materials. This includes embedded magnetic nanostructures, which are accessible due to the large penetration depth of optical radiation. The linear magneto-optic Kerr effect is widely used in the growth and characterization of ultra-thin magnetic films and can show monolayer sensitivity. Nonlinear magnetic second-harmonic generation (MSHG) is a more difficult and expensive technique but, uniquely, can measure the surface and interface magnetism of centrosymmetric magnetic films with sub-monolayer sensitivity. MSHG is briefly reviewed and examples from high symmetry interfaces and nanostructures described. Low symmetry structures are more difficult to characterize, however, because of the large number of tensor components that may contribute to the signal. An important class of low symmetry systems exploits vicinal substrates to grow aligned magnetic nanostructures by self-organization. These structures have a high proportion of magnetic step or edge atoms relative to the terrace atoms, and the overall magnetic response is expected to contain significant contributions from these different magnetic regions. It is shown that contributions from these different regions can be identified using normal

incidence (NI) MSHG. This new approach is used to determine hysteresis loops from Au-capped Fe monolayers grown on a vicinal W(110) substrate. Temperature-dependent studies of the MSHG contrast also allow Curie temperatures to be determined. This experimental procedure and phenomenology opens up low symmetry magnetic interfaces and aligned nanostructures to characterization by MSHG.

PACS 75.70.Ak, 75.70.Cn, 42.65.Ky

Keywords: Magnetic, interface, optics, second-harmonic, iron, tungsten, nanostructure, step, terrace

1. Introduction

Magnetic interfaces and nanostructures are attracting considerable current interest, both regarding the fundamental physics and in their technological application [1]. In the sub-monolayer regime, self-assembly at atomic steps has been used to grow aligned, model nanostructures. For example, Fe nanostripes have been grown on vicinal W(110) and their magnetic behaviour has been probed using the magneto-optic Kerr effect (MOKE) [2, 3], while x-ray magnetic circular dichroism (XMCD) has been used to identify ferromagnetism in single atomic wires of Co grown on Pt(997) [4, 5]. A key advantage of these photon-in/photon-out techniques, apart from their sensitivity, is their ability to probe buried nanostructures located in the interfacial region between the substrate and the capping layer used to protect the nanostructure from environmental corrosion and contamination [6]. However, techniques such as MOKE and XMCD have difficulty in discriminating between bulk and interface effects, or between interface and step contributions in aligned magnetic nanostructures.

Nonlinear optical techniques, such as optical second-harmonic generation (SHG), use symmetry to discriminate between the interfacial contribution and the normally dominant bulk response, allowing the interfacial structure of centrosymmetric systems to be determined [7]. Magnetic SHG (MSHG) extends this approach to magnetic interfaces. It was realised that magnetization, as an axial vector, did not lift the inversion symmetry of the bulk, allowing magnetic surfaces and interfaces to be probed [8, 9]. The first experimental results soon appeared [10] and, with the development of reliable femtosecond lasers, MSHG surface and interface studies became relatively straightforward, due to the improvement in the signal-to-noise ratio (SNR).

Within the electric dipole approximation, the intensity of MSHG from a magnetic interface is given by

$$I(2\omega;\pm\boldsymbol{M}) \propto |\boldsymbol{\chi}^{\boldsymbol{eff}}_{\boldsymbol{even}}\boldsymbol{E}(\omega)\boldsymbol{E}(\omega) \pm \boldsymbol{\chi}^{\boldsymbol{eff}}_{\boldsymbol{odd}}\boldsymbol{M}\,\boldsymbol{E}(\omega)\boldsymbol{E}(\omega)|^2 \quad (1)$$

where $\boldsymbol{\chi}^{\boldsymbol{eff}}_{\boldsymbol{even}}$ is the effective third rank crystallographic susceptibility tensor, $\boldsymbol{E}(\omega)$ is the input electric field vector, $\boldsymbol{\chi}^{\boldsymbol{eff}}_{\boldsymbol{odd}}$ is the effective fourth rank axial magnetic susceptibility tensor, and $\boldsymbol{M}$ is the interface magnetization [9]. Higher order quadrupolar crystallographic contributions from the substrate or capping layer can be included in the effective value of the *even* term. SHG is known to be sensitive to strain [11] and any magneto-elastic contributions will appear in the *even* term [12]. Appropriate Fresnel and local electromagnetic field factors [13] are included in the effective tensor components of Eq. (1).

A comprehensive review of MSHG has been published recently by Kirilyuk and Rasing [14] and only a few important examples will be highlighted here. Compared to SHG, new *odd* magnetic tensor components have appeared, giving a contribution to the MSHG intensity that changes sign with the magnetization. The crystallographic terms are *even* in the magnetization, as shown in Eq. (1). This analysis was elegantly confirmed when an optical phase shift of 180^o in the SH signal was measured on reversing the magnetization in a Rh/Co/Cu multilayer [15]. Hysteresis loops in the MSHG intensity have been measured for different magnetic surface and interfaces. The Cu(001)/Fe system shows 4x1 and 5x1 reconstructions below 4 monolayers (ML) coverage, and a 2x1 reconstruction above 4 ML. Very different surface hysteresis loops for these two phases were found (Fig. 1), and coverage dependent studies up to 12 ML were used to show that there was no bulk contribution to the MSHG signal [16]. Other important experiments include the *in situ* measurement of oscillations in the MSHG intensity during the growth of Co and Fe films [17, 18]. In the latter case a monolayer of oxygen acts as a surfactant in the

homoepitaxial growth of Fe films on Fe(001), floating on the top of the growing film. The oscillations in MSHG intensity (Fig. 2) were attributed to the 7% outward relaxation of the top Fe layer, which is expected to increase the magnetic moment of the Fe atoms [18]. *Ex situ* MSHG and MOKE oscillations have been observed from an exchange biased Co wedge, grown layer-by-layer on Cu(001) from 9 to 13 ML coverage, and capped with a 25 ML Mn film [19]. Coercivities determined from the MSHG and MOKE measurements oscillate in phase (Fig. 3), indicating that the bulk and interface magnetization change in the same way with field reversal. The MSHG asymmetry or contrast was used to infer that the net magnetic moment at the interface was enhanced at monolayer completion. Assuming that the effective *odd* contribution is relatively small compared to the *even* contribution, the expression for the MSHG contrast can be linearized:

$$A = \frac{I^+ - I^-}{I^+ + I^-} \approx 2\frac{|\chi_{odd}^{eff} M|}{|\chi_{even}^{eff}|}\cos\theta \qquad (2)$$

where the +/- superscript refers to equal but opposite magnetizations, and θ is the phase difference between the *odd* and *even* components [16, 18, 19]. It can be seen from Eq. (2) that, if the effective *even* and *odd* components either remain constant, or vary in the same way, in an experiment, the asymmetry is proportional to the magnetization. For example, the main contributions to variation in the tensor components with coverage are expected to come from changes in the local electronic structure and the local electromagnetic fields at the interface. It was pointed out that the edge or step contributions are likely to be different to those of the islands

or terrace [19]. Indeed, MOKE studies from magnetic films grown on vicinal substrates have reported distinct step effects at higher vicinal angles [20-22].

2. Extension to aligned nanostructures

Step or edge contributions are expected to become increasingly important in the magnetization behaviour of aligned magnetic nanostructures as their dimensions shrink. Self-assembly at atomic steps on vicinal single crystal surfaces has proved to be a useful route to aligned structures, with two well studied systems being vicinal W(110)/Fe, where MOKE was used to measure the magnetization of sub-monolayer nanostripes as small as 10 atoms in width [2], and Pt(997)/Co, where the magnetization of single atomic wires was measured using XMCD [4]. A major attraction of applying MSHG to aligned magnetic nanostructures is that the symmetry of the edges or steps is lower than that of the terraces or islands and this, in principle, allows their contribution to the response of the system to be distinguished by MSHG [23]. However, two major difficulties must first be overcome: sensitivity and complexity.

One approach to overcoming the former is to account properly for the quadratic magnetic response implicit in Eq. (1), rather than choosing an experimental configuration that produces a smaller magnetic response in order to allow Eq. (1) to be linearized [24]. It may also be difficult to judge whether quadratic terms are distorting the loops in exchange biased systems, where loops may be acentric. Fig. 4 shows a comparison of MOKE and SHG results from an exchange biased system, where it was pointed out that the difference may be due to quadratic effects [25]. Without this constraint, a large value of the asymmetry can be chosen, which increases the SNR. Fig. 5 shows that, for 3 ML Fe, the quadratic term introduces turning points in the MSHG

response, but that this can be dealt with using two different approaches and the magnetic hysteresis loop successfully extracted [24].

The difficulties arising from the complexity of the nonlinear response have been largely avoided by restricting studies to magnetic thin film systems of high surface and interface symmetry [14]. Lower symmetry systems, which may have multiple magnetic regions, have many tensor components that may contribute to the MSHG intensity, making interpretation particularly difficult. Recently, a new approach to MSHG studies of lower symmetry systems has been developed and applied to the vicinal W(110)/Fe system, capped with Au [26]: normal incidence (NI) SHG geometry simplifies the nonlinear response from systems of lower symmetry by excluding *z*-dependent tensor components.

In this paper it is shown that fine tuning of the input polarization direction can enhance the magnetic contribution to the NI SHG signal, resulting in a significant improvement in the SNR of hysteresis loops extracted from the measurements. It is also shown that the improved SNR allows the presence of different magnetic regions at the inhomogeneous interface to be identified by changing the input polarization direction, which alters relative contribution of the tensor components to the overall NI MSHG response.

3. NI MSHG from magnetic interfaces and nanostructures of 1m symmetry

In general, low symmetry magnetic interfaces and nanostructures are inhomogeneous, containing two or more regions where the same magnetic species is found with a different number of magnetic and non-magnetic nearest neighbours. Since the magnetic properties of an interface are known to depend sensitively on nearest neighbour number and type [27], a full description of NI MSHG from an inhomogeneous interface must account for the contributions made by the different regions. It has been shown for NI MSHG that, through careful choice of

sample alignment with respect to output polarization selection and the direction of applied magnetic field, the contribution from each region can be reduced to one *even* crystallographic tensor component and two *odd* magnetic tensor components [23].

The third rank crystallographic tensor components and fourth rank magnetic tensor components in Eq. (1) are expressed using the simplified notation $\chi_{ijk} \equiv ijk$ and $\chi_{ijkL} \equiv ijkL$, respectively, where the upper-case subscript *L*, describing the magnetization direction, is introduced to avoid potential confusion with unrelated quadrupolar susceptibility tensor components [14]. The interface formed by the pseudomorphic deposition of a magnetic species on a vicinal surface, consisting of well-ordered 1m atomic steps separated by higher symmetry surface terraces or islands, possesses overall 1m symmetry. If the surface normal of the interface is in the *z*-direction, the normal to the single mirror-plane is in the *y*-direction along the steps, and the magnetization is in the *x*-direction (M_X), then the *y*-polarized NI MSHG intensity probes only the three tensor components, yxy, $yxxX$ and $yyyX$ [23]. For different magnetic regions, *n*, the dependence of the *y*-polarized NI MSHG intensity on φ, the angle between the input polarization field and the *x*-direction, is given by:

$$I_y(2\omega; \varphi, \pm M_X) \propto |\sum_n yxy^{(n)} \sin 2\varphi \pm \{yxxX^{(n)} \cos^2\varphi + yyyX^{(n)} \sin^2\varphi\} M_X^{(n)}|^2 \qquad (3)$$

MSHG thus offers the important diagnostic capability of exploiting the properties of the optical tensor components to identify different magnetization contributions from inhomogeneous interfaces and nanostructures, because the components will vary with the local atomic structure.

For centrosymmetric magnetic hysteresis loops, further simplification of Eq. (3) occurs on eliminating the quadratic contribution using the Type II procedure of Ref. [24]:

$$\begin{aligned}\Delta I_y^{\pm}(2\omega;\varphi,H) &\equiv I^{\pm}(2\omega;\varphi,H) - I^{\mp}(2\omega;\varphi,-H) \\ &\propto 4\sin 2\varphi \cos^2\varphi \sum_{n,n'} |yxy^{(n)}||yxxX^{(n')}| \cos(\Delta\theta_{yx}^{nn'}) M_X^{\pm(n')} \\ &+ 4\sin 2\varphi \sin^2\varphi \sum_{n,n'} |yxy^{(n)}||yyyX^{(n')}| \cos(\Delta\theta_{yy}^{nn'}) M_X^{\pm(n')}\end{aligned} \quad (4)$$

where I^+ has H increasing from an initial negative value, and I^- has H decreasing from an initial positive value, and $\Delta\theta_{yi}^{nn'} = \theta_{yxy}^{n} - \theta_{yiiX}^{n'}$, where θ are the complex phase factors of the tensor components. This procedure removes all terms even in the magnetization, including magneto-elastic terms and cross-terms in the magnetization from different regions. It can be seen from Eq. (4) that choosing φ close to 0° or 90° will limit the magnetic contributions to a single component per region, $yxxX^{(n')}$ and $yyyX^{(n')}$, respectively.

As well as producing the much simplified Eq. (4), NI geometry has the advantage of eliminating any isotropic capping layer contribution to the *even* term, and thus also to the phase difference between the *even* and *odd* components. If the surface of the capping layer is macroscopically isotropic, as is often the case where no special effort is made to grow an epitaxial capping layer, then NI ensures no contribution to the *even* terms from the surface of the cap.

This much simplified equation can be fitted, for example, using normalized sigmoidal magnetization loops of the form:

$$M^{(n)+}(H) = -1 + 2/\{1 + \exp[-s^{(n)}(H - H_c^{(n)})]\} \tag{5}$$

where $s^{(n)}$ is the softness and $H_c^{(n)}$ the coercivity of the n^{th} loop. Only the magnetization depends on the applied magnetic field in Eq. (4), with the remaining terms determining the scale of the measured response. In the absence of other information, this prevents the strength of the magnetization being determined, but the softness and coercivity are unaffected by these scaling factors.

The full expression for the magnetic contrast or asymmetry is more complicated and, for φ close to 0° or 90° (and symmetry related angles), is given by:

$$A_{\varphi\approx 0} \equiv \frac{I_y^+ - I_y^-}{I_y^+ + I_y^-} = \frac{4\varphi \sum_{n,n'} |yxy^{(n)}||yxxX^{(n')}| \cos(\Delta\theta_{xx}^{nn'}) M^{(n')}}{4\varphi^2 \sum_{n,n'} |yxy^{(n)}||yxy^{(n')}| \cos(\Delta\theta_{yxy}^{nn'}) + \sum_{n,n'} |yxxX^{(n)}||yxxX^{(n')}| \cos(\Delta\theta_{yxxX}^{nn'}) M^{(n)} M^{(n')}} \tag{6}$$

$$A_{\varphi\approx \pi/2} = \frac{4(\frac{\pi}{2} - \varphi) \sum_{n,n'} |yxy^{(n)}||yyyX^{(n')}| \cos(\Delta\theta_{yy}^{nn'}) M^{(n')}}{4(\frac{\pi}{2} - \varphi)^2 \sum_{n,n'} |yxy^{(n)}||yxy^{(n')}| \cos(\Delta\theta_{yxy}^{nn'}) + \sum_{n,n'} |yyyX^{(n)}||yyyX^{(n')}| \cos(\Delta\theta_{yyyX}^{nn'}) M^{(n)} M^{(n')}} \tag{7}$$

The asymmetry is expected to be useful in investigating temperature dependent behaviour, which is not straightforward. Equations (6) and (7) show that, as long as the temperature variation of the components is similar, then substantial cancellation will occur in the asymmetry expression.

5. Hysteresis loops and Curie curves from Au-capped Fe nanostructures grown on vicinal W(110)

Buried magnetic nanostructures, when formed by adsorption of magnetic material on non-magnetic substrates of 1m symmetry and then capped by non-magnetic material, are generally inhomogeneous, with *n* distinct magnetic regions, where the same magnetic element is found with different numbers of magnetic, substrate, and capping layer nearest neighbours. For Fe deposition on 1.4° vicinal W(110), it is well known that Fe nanostripes are formed running parallel to the step edges, with an in-plane easy axis of magnetization orthogonal to the steps. The width of the stripes increases with further deposition until the (110) terraces are fully covered [2]. This growth mode continues to about 2 ML [28] but, at higher coverage, Stranski-Krastanov growth occurs, with large Fe islands being formed, at least ten atomic layers thick, on a pseudomorphic Fe monolayer [29]. In addition, it is well established that capping such Fe layers with Au at room temperature does not produce any inter-diffusion or reaction [3].

Both the magnetization [27, 30], and the nonlinear optical susceptibility [17], in the interfacial region are known to depend sensitively on the type and number of nearest neighbours. For *y*-polarized NI MSHG from this type of vicinal system, symmetry allows all 1m (step) regions and 2mm (terrace) regions to contribute to the *odd* magnetic contribution, but excludes *even* crystallographic tensor components from regions of 2mm symmetry [23]. The normally dominant contributions from the *even* terms are thus much reduced by this choice of geometry, enhancing the sensitivity of the measurement to the magnetization.

Preparation of the Au-capped ultra-thin Fe films has been described in detail elsewhere [31]. Briefly, Fe films were grown under ultra-high vacuum conditions on a clean vicinal W(110) single crystal substrate, offcut 1.4° in the $[1\bar{1}0]$ (x) direction, which produces atomic steps running in the [001] (y) direction. The Fe films were protected by a 12 to16 nm thick, optically isotropic, capping layer of Au, deposited at room temperature. The capped samples were placed in an optical cryostat and the MSHG hysteresis loops were measured at 80 K with the applied magnetic field aligned along the $[1\bar{1}0]$ easy axis at two different input polarization angles, φ, close to 0° and 90° (or symmetry-related positions [26]). The variation in the magnetic asymmetry with temperature was also measured, at saturation, from 80 K to room temperature. A femtosecond laser, tuned to ~1.5 eV, was used at near normal incidence, with the output polarizer aligned such that SH electric field vector lies in the surface plane parallel to the steps. Unamplified 130 fs Ti:sapphire laser pulses, of average power of 0.9W, were used at a repetition rate of 76 MHz. The beam size at the sample was 40 μm.

Two examples of the application of Eqs (4)-(7) are shown in Figure 6 for 0.25 ML and 3 ML coverage. It can be seen that this new MSHG approach is sensitive to as little as 0.25 ML Fe coverage for this material system, even for unamplified pulses. Solid lines are simultaneous fits, for a given coverage, to the extracted loop data (upper row) and the magnetic contrast data (lower row). This allows the coercivity, softness, and Curie temperature of different regions to be estimated. The magnetization (y) axis of the extracted loops scales with the experimental data, but is otherwise arbitrary. The SNR for unamplified pulses is not sufficient to determine the shape of the Curie curves for this material system. The shape is approximated by a Fermi function here in order to estimate the Curie temperature at half the saturation magnetization [32].

For 0.25 ML coverage, the ~10 atom wide Fe stripes have a coercivity of 3(5) mT, a softness of 0.07(3), and a Curie temperature, T_C, of 139(10) K, where estimated errors are given in parenthesis. The relatively narrow transition is consistent with dipolar coupling between the stripes [2]. Pratzer and Elmers, in studying the same system using MOKE, found a T_C value of 115(10) K for 0.3 ML Fe, capped by 6 ML of Au (Fig. 4 of Ref. [3]). However, in this work the T_C value is defined at vanishing remanence, increasing the discrepancy by about 10 K. It is possible that the different capping layer thicknesses account for this difference in T_C [33].

For 3 ML coverage, where large Fe islands are formed on a pseudomorphic Fe monolayer, two magnetic regions can be identified from the extracted loops. Region 1 has a coercivity of 18(5) mT, a softness of 0.25(3), and a T_C value of 180(10) K, while Region 2 has a coercivity of 38(5) mT, a softness of 0.17(3), and a T_C value of 294(10) K. The large variation in loop width in Fig. 6 clearly shows the presence of more than one magnetic region. It is of note that the extracted curves are centrosymmetric within experimental error, thus excluding any significant magneto-elastic contribution.

The terrace interface regions are expected to dominate the response at this higher coverage, as the morphology results in only a small proportion of step or edge atoms. Possible contributions come from the Fe/Au interface at the top of the large, ~10 atomic layer islands, the W/Fe/Au interface at the pseudomorphic monolayer, and the W/Fe interface beneath the islands. The fitting procedure for this coverage gives a phase shift of ~180° between the two regions for the dominant yyyX component, which indicates that the lower island interface is one of the contributing regions, with the other likely to be the upper island interface, although the pseudomorphic Fe monolayer between the islands cannot be ruled out. The different local electronic structure of these interfaces means that they are not exact mirror images of each other and so the phase shift will not produce full cancellation of the response. Further evidence for this

interpretation is that capping this material system with Au is known to increase the coercivity significantly [3], which is consistent with the quite different values obtained for the two regions.

The temperature variation of the contrast requires two conventional Curie curves to enable the region below 200 K to be fitted, where the contrast is clearly increasing with temperature (Fig. 6). This is consistent with the two yyyX components being out of phase, as mentioned above. As the temperature increases above the lower Curie temperature of 180(10) K, the partial cancellation is removed, resulting in an increase in contrast. While it is possible that this behaviour may be due to incomplete cancellation of the temperature variation of the tensor components, or a two-phase-like inflection found in some inhomogeneous magnets [34], it is interesting to consider the possibility that there are, indeed, two Curie temperatures being measured, associated with the upper and lower interfaces. The correlation length of the exchange interaction can be comparable to the interatomic spacing where the two contributing regions have very different values of T_C [35]. Spin-polarized electron scattering studies have reported a bulk T_C value of ~500 K above 2 ML Fe coverage on singular W(110) [36]. The interface T_C values of 180(10) K and 294(10) K are sufficiently far from 500 K that the mean field exchange correlation length [35] reduces to below the interatomic distance. While this is based on a relatively simple three-dimensional model, it does provide support for the idea that different Curie temperatures may exist in regions such as interfaces, steps and edges, where the local electronic and magneto-crystalline anisotropy differs significantly from the bulk. This deserves further exploration, as it has interesting technological implications.

5. Conclusion

Nonlinear magnetic second-harmonic generation (MSHG), which can measure the surface and interface magnetism of centrosymmetric magnetic films with sub-monolayer sensitivity, has

been briefly reviewed and examples from high symmetry interfaces and nanostructures described. Low symmetry structures are more difficult to characterize, however, because of the large number of tensor components that may contribute to the signal. Aligned magnetic nanostructures have a high proportion of magnetic step or edge atoms relative to the terrace atoms, and the overall magnetic response is expected to contain significant contributions from the different magnetic regions. It has been shown that these different regions can be identified using normal incidence MSHG. The new approach has been used to determine hysteresis loops from Au-capped Fe monolayers grown on a vicinal W(110) substrate. Temperature-dependent studies of the MSHG contrast have allowed Curie temperatures to be determined. This experimental procedure and phenomenology opens up low symmetry magnetic interfaces and aligned nanostructures to characterization by MSHG.

Acknowledgments

This publication has emanated from research conducted with the financial support of Science Foundation Ireland, the Irish Higher Education Authority and the Irish Research Council for Science, Engineering and Technology.

References

[1] J. P. Velev, P. A. Dowben, E. Y. Tsymbal, S. J. Jenkins, and A. N. Caruso, Surf. Sci. Rep. 63 (2008) 400.
[2] J. Hauschild, H. J. Elmers, and U. Gradmann, Phys. Rev. B 57 (1998) R677.
[3] M. Pratzer and H. J. Elmers, Phys. Rev. B 67 (2003) 94416.
[4] P. Gambardella, A. Dallmeyer, K. Malti, M. C. Malagoli, W. Eberhardt, K. Kern, and C. Carbone, Nature 416 (2002) 301.
[5] P. Gambardella, A. Dallmeyer, K. Maiti, M. C. Malagoli, S. Rusponi, P. Ohresser, W. Eberhardt, C. Carbone, and K. Kern, Phys. Rev. Lett. 93 (2004) 077203.
[6] J. F. McGilp, Prog. Surf. Sci. 49 (1995) 1.
[7] Y. R. Shen, Nature 337 (1989) 519.
[8] S. B. Borisov and I. L. Lyubchanskii, Optics and Spectroscopy 61 (1986) 801.
[9] R.-P. Pan, H. D. Wei, and Y. R. Shen, Phys. Rev. B 39 (1989) 1229.
[10] J. Reif, C. Zink, C. M. Schneider, and J. Kirschner, Phys. Rev. Lett. 67 (1991) 2878.
[11] J.-W. Jeong, S.-C. Shin, I. L. Lyubchanskii, and V. N. Varyukhin, Phys. Rev. B 62 (2000) 13455.
[12] E. du Tremolet de Lacheisserie, Phys. Rev. B 51 (1995) 15925.
[13] Y. R. Shen, The Principles of Nonlinear Optics, Wiley, New York, 1984.
[14] A. Kirilyuk and T. Rasing, J. Opt. Soc. Am. B 22 (2005) 148.
[15] K. J. Veenstra, A. V. Petukhov, A. P. De Boer, and T. Rasing, Phys. Rev. B 58 (1998) R16020.
[16] M. Straub, R. Vollmer, and J. Kirschner, Phys. Rev. Lett. 77 (1996) 743.
[17] Q. Y. Jin, H. Regensburger, R. Vollmer, and J. Kirschner, Phys. Rev. Lett. 80 (1998) 4056.
[18] M. Nyvlt, F. Bisio, J. Franta, C. L. Gao, H. Petek, and J. Kirschner, Phys. Rev. Lett. 95 (2005) 127201.
[19] V. K. Valev, A. Kirilyuk, F. D. Longa, J. T. Kohlhepp, B. Koopmans, and T. Rasing, Phys. Rev. B 75 (2007) 012401.
[20] H. J. Choi, Z. Q. Qiu, J. Pearson, J. S. Jiang, D. Li, and S. D. Bader, Phys. Rev. B 57 (1998) 12713.
[21] H. J. Choi, R. K. Kawakami, E. J. Escorcia-Aparicio, Z. Q. Qiu, J. Pearson, J. S. Jiang, L. Dongqi, and S. D. Bader, Phys. Rev. Lett. 82 (1999) 1947.
[22] H. J. Choi, R. K. Kawakami, E. J. Escorcia-Aparicio, Z. Q. Qiu, J. Pearson, J. S. Jiang, D. Li, R. M. Osgood, III, and S. D. Bader, J. Appl. Phys. 85 (1999) 4958.
[23] L. Carroll and J. F. McGilp, phys. stat. sol. (c) 0 (2003) 3046.
[24] J. F. McGilp, L. Carroll, and K. Fleischer, J. Phys.: Condens. Matter 19 (2007) 396002.
[25] V. K. Valev, M. Gruyters, A. Kirilyuk, and T. Rasing, phys. stat. sol. (b) 242 (2005) 3027.
[26] L. Carroll, K. Fleischer, J. P. Cunniffe, and J. F. McGilp, J. Phys.: Condens. Matter 20 (2008) 265002.
[27] H. J. Elmers, Int. J. Mod. Phys. B 9 (1995) 3115.
[28] J. Hauschild, U. Gradmann, and H. J. Elmers, Appl. Phys. Lett. 72 (1998) 3211.
[29] M. Bode, A. Wachowiak, J. Wiebe, A. Kubetzka, M. Morgenstern, and R. Wiesendanger, Appl. Phys. Lett. 84 (2004) 948.

[30] D. Repetto, T. Y. Lee, S. Rusponi, J. Honolka, K. Kuhnke, V. Sessi, U. Starke, H. Brune, P. Gambardella, C. Carbone, A. Enders, and K. Kern, Phys. Rev. B 74 (2006) 54408.
[31] K. Fleischer, L. Carroll, C. Smith, and J. F. McGilp, J. Phys.: Condens. Matter 19 (2007) 266003.
[32] E. V. Albano, K. Binder, D. W. Heermann, and W. Paul, Zeit. Phys. B 77 (1989) 445.
[33] M. Pajda, J. Kudrnovsky, I. Turek, V. Drchal, and P. Bruno, Phys. Rev. Lett. 85 (2000) 5424.
[34] R. Skomski, J. Phys.: Condens. Matter 15 (2003) 841.
[35] R. Skomski and D. J. Sellmyer, J. Appl. Phys. 87 (2000) 4756.
[36] H. J. Elmers, J. Hauschild, H. Fritzsche, G. Liu, U. Gradmann, and U. Kohler, Phys. Rev. Lett. 75 (1995) 2031.

Fig. 1

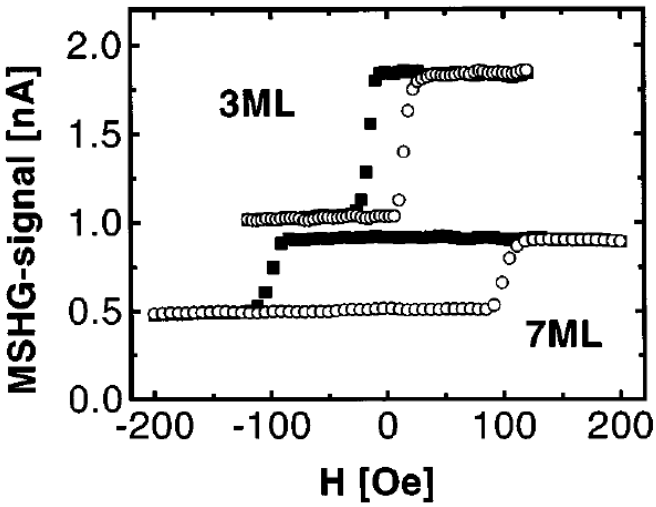

Fig. 2

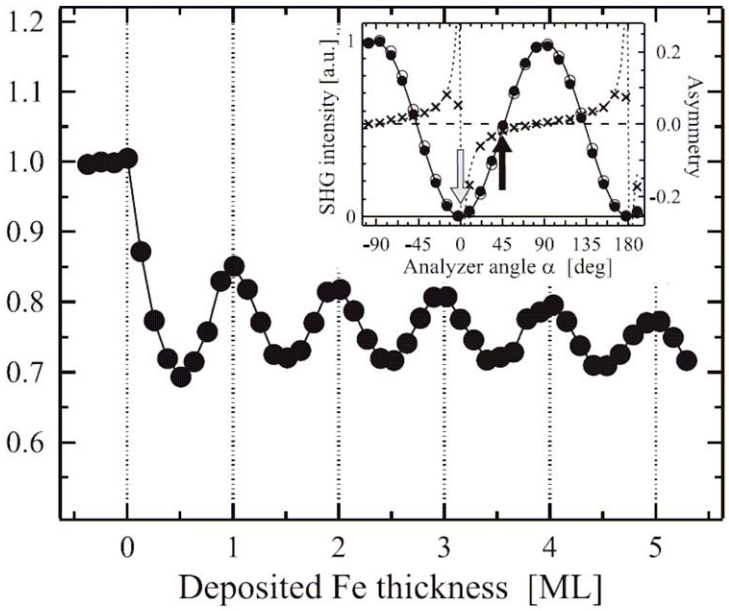

Fig. 3

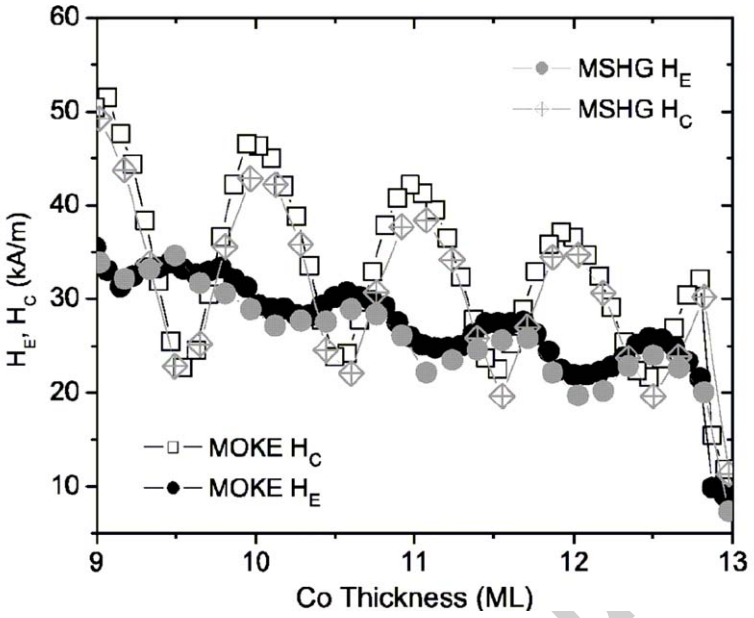

Fig. 4

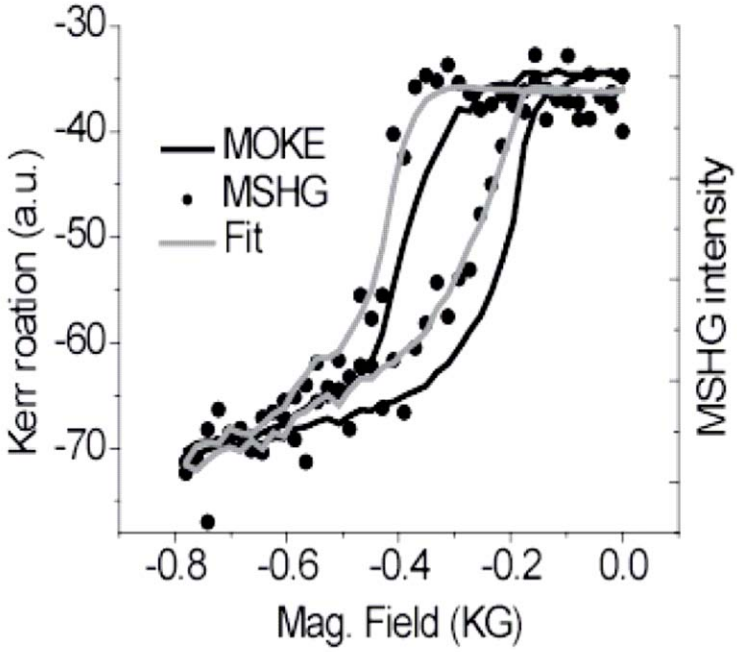

Fig. 5

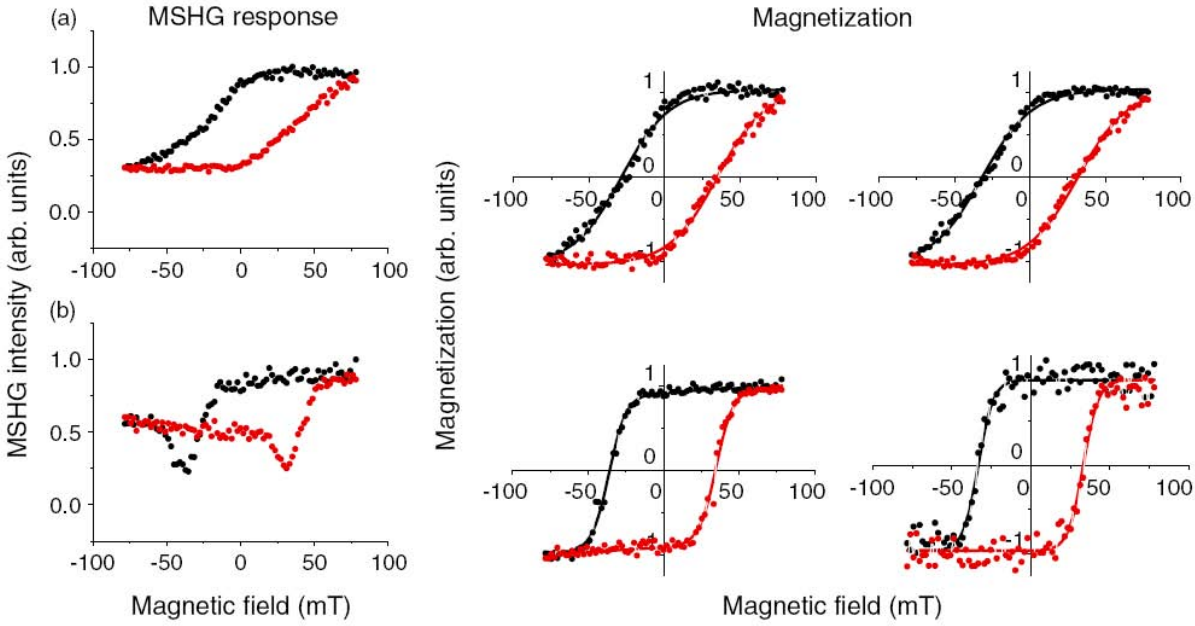

Fig. 6

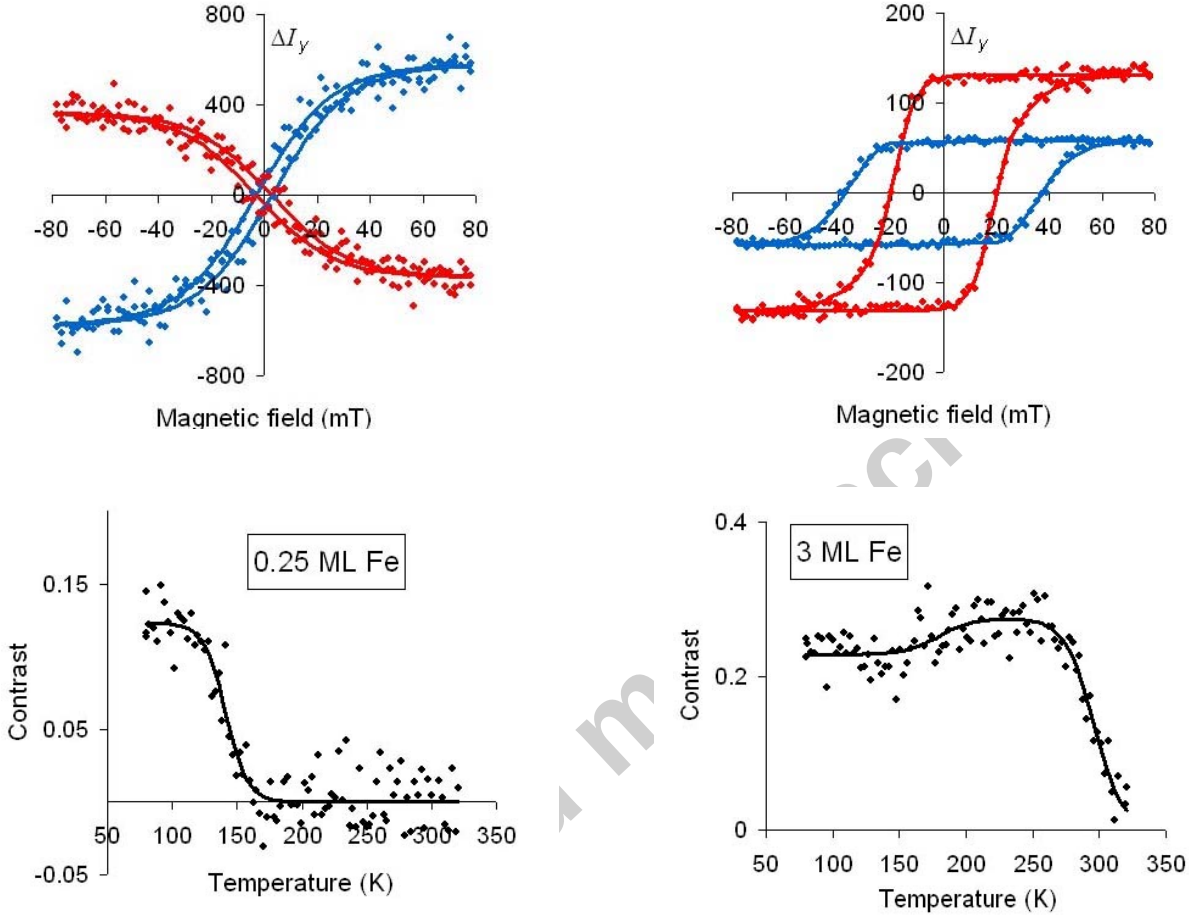
800
400
0
-400
-800
ΔI_y
-80 -60 -40 -20 0 20 40 60 80
Magnetic field (mT)
200
100
0
-100
-200
ΔI_y
-80 -60 -40 -20 0 20 40 60 80
Magnetic field (mT)
0.25 ML Fe
0.15
0.05
-0.05
Contrast
50 100 150 200 250 300 350
Temperature (K)
3 ML Fe
0.4
0.2
0
Contrast
50 100 150 200 250 300 350
Temperature (K)

Legends

Fig. 1. MSHG hysteresis loops for 3 ML and 7 ML Fe on Cu(001) (after [16]).

Fig. 2. Normalized effective odd component amplitude for p-in/s-out geometry, as a function of the deposited Fe thickness on Fe(001)-1x1-O.. Inset: SHG intensities, I^+(open circles) and I^- (solid circles), and asymmetry, A (crosses) as a function of the analyzer angle, α, for p-in fundamental light. The p-in/s-out and p-in/sp-out geometries are indicated by the gray and black arrows (after [18]).

Fig. 3. Coercivity and exchange bias of the hysteresis curves from MSHG ‖in gray| and MOKE ‖in black| as function of the Co thickness (after [19]).

Fig. 4. Simultaneous MOKE (black line) and MSHG (dots) measurements of an exchange biased Si(111)/6 nm Fe/2 nm CoO/6 nm Au sample at 50 K. The grey line is a numerical fit for the MSHG intensity data (after [25]).

Fig. 5. MSHG data for vicinal W(110)/Fe nanostructures, capped with ~15 nm Au. Left panels: MSHG response for (a) 0.75ML Fe, (b) 3ML Fe. Centre panels: extracted magnetization loops using a general approach that accounts for the quadratic contribution. Right panels: extracted loops assuming a centrosymmetric magnetic response. Solid lines are fits to the extracted loops using sigmoidal curves (after [24]).

Fig. 6. Extracted centrosymmetric loops for input polarization angles near 0° and 90° (or symmetry-related positions), together with the magnetic contrast as a function of temperature. Solid lines are simultaneous fits to all sets of data for a given coverage, using the equations in the text. Left column: 0.25 ML Fe. Right column: 3 ML Fe.